Lattice dynamics of Kr films on the graphite (0001) surface by inelastic helium-atom scattering

Jinhe Cui, David R. Jung, and Renee D. Diehl
The Pennsylvania State University, University Park, Pennsylvania 16802
(Received 3 May 1991; revised manuscript received 8 November 1991)

Lattice dynamics of the Kr monolayer, bilayer, and trilayer physisorbed on graphite (0001) surface were studied by inelastic He-atom scattering ($k_i = 5.77$ Å^{-1}). The out-of-plane vibrational mode of the monolayer along both the $\bar{\Gamma}\bar{M}_R$ and $\bar{\Gamma}\bar{K}_R$ symmetry directions is essentially dispersionless with vibrational energy of 4.1 meV for $Q \geq 0.3$ Å^{-1}. For $Q \leq 0.3$ Å^{-1}, a strong interaction between adsorbate and substrate was indicated by the observation of an avoided-crossing behavior in the disperison curve and anomalous intensity distributions in the time-of-flight spectra. The disperison curves of the bilayer and trilayer, which are much lower in energy than that of the monolayer, appear to be the same and are not perturbed significantly by the substrate.

I. INTRODUCTION

Physisorbed films of rare gases on graphite have been studied extensively in the past two decades.[1-6] Unlike most other substrates used for the study of physisorbed and chemisorbed films, the graphite surface has a large corrugation in its holding potential which leads to a wide diversity of structures and phase transitions. To date, most experimental studies on the adsorbed films on graphite have only been concerned with static information such as structure, ordering, wetting, and equilibrium phase transitions. The lattice dynamics of adsorbed layers has been the subject of relatively little experimental work in spite of its importance in understanding the adsorbate-substrate and adsorbate-adsorbate interaction potentials.

The lattice dynamics of a rare-gas adlayer on smooth surfaces is predicted to be influenced by the coupling between adsorbate and substrate.[7] Two major effects are expected to occur when the dispersion curve of the adlayer $SP_\perp$ mode, which is polarized along the surface normal, crosses those of the surface and bulk phonon modes of the substrate. One is the hybridization of the adlayer mode and the Rayleigh mode of the substrate and the other is the resonance-induced lifetime broadening of the adlayer mode.[7] The effects are expected to be strongest for the monolayer and decreasingly smaller as the film becomes thicker. A number of experimental studies have been performed by inelastic He-atom scattering for rare-gas adlayers on close-packed metal surfaces[8-11] and also for monolayer Xe on the graphite surface.[12] These studies indicate that, on the metal surfaces, the adlayer phonon modes couple only weakly with the substrate, although effects of both hybridization and lifetime broadening were observed in the system of Kr/Pt(111).[11] In contrast, the lattice-dynamics measurements of monolayer Xe on graphite show a much stronger coupling between adlayer and substrate phonon modes, as indicated by the observation of a large splitting in the dispersion curve due to the hybridization of adlayer and substrate phonon modes.[12] These measurements clearly demonstrated that the inelastic He-atom scattering can provide detailed information on the adsorbate-substrate interaction, which is very important for understanding the behavior of physisorbed films.

In this paper we describe our inelastic He-atom scattering measurements of the lattice dynamics of monolayer, bilayer, and trilayer Kr adsorbed on the basal plane of a graphite single crystal. This is part of a systematic and continuing effort in the laboratory to study the interaction potential, structure,[13] commensurate-incommensurate phase transition,[14] and lattice dynamics of this system. A strong interaction between adsorbate and substrate vibrational modes was observed in the monolayer. The effect of such an interaction, however, was found to be much less important for the bilayer and trilayer.

II. EXPERIMENT

A. Apparatus and experimental method

Details of our apparatus have been described before.[15] A nearly monochromatic ($\Delta v/v = 1\%$) low-energy He beam is produced by expanding high-pressure (300 psi) thermal He gas through a 7.5-μm nozzle cooled by liquid nitrogen. Before entering the scattering chamber the beam is modulated at a frequency of 120 Hz by a rim-type mechanical chopper[16] which has several equally spaced slots 0.02 in. wide. The time width of the pulses, determined from the time-of-flight (TOF) spectrum of specular reflection from the bare graphite surface, is about 28 μs, which corresponds to an energy uncertainty of 0.9 meV. The angular divergence of the incident beam is about 0.1°, and the diameter of the beam at the position of the sample is about 1.4 mm. The scattered He atoms were detected in the in-plane scattering geometry with total scattering angle fixed at 90° by a magnetic mass spectrometer residing in the last of four differential pumping stages.

A natural graphite single crystal (extracted from a Ticonderoga, NY, are kindly supplied by T. S. Noggle of Oak Ridge National Laboratory), which is about 0.5 mm thick and 4 mm in diameter, was cleaved in air with a

piece of adhesive tape. The crystal was then clamped onto the sample rocker plate by a 0.5-mm-thick copper mask. The sample rocker plate is thermally linked by six copper braids to the cold finger of a closed-cycle refrigerator. This allows cooling the sample to 35 K while maintaining azimuthal rotation and tilt freedom as well. The temperature of the sample is measured by a calibrated platinum thermometer clamped on the rocker plate. The uncertainty in temperature measurements is about 1.5 K in the temperature range of 35–300 K, and is mostly due to the uncertainty in the calibration process. A homemade heater residing behind the copper rocker plate provides the capability of heating the sample up to 700 K by means of electron bombardment and radiation. The scattering chamber is pumped by a 600 l/s cyropump, with a titanium sublimation pump in parallel. The base pressure in the chamber is about 3×10^{-10} torr and rises to 4.5×10^{-10} torr when the He beam is on. To clean the graphite surface the sample was heated in ultrahigh vacuum to 650 K for about 10 h prior to any experimental measurements. A clean and ordered surface is indicated by the observation of an intense He reflection from the surface. At surface temperatures near 60 K, peak intensities of 2 MHz and 150 kHz (compared with 20 MHz for the incident beam) are typically observed for specular and first-order diffraction beams with angular widths of 0.3° and 0.6°, respectively. The observed angular widths of these beams, however, are much wider than those due to instrumental broadening, which are 0.15° for the specular and 0.35° for the diffraction beams. This extra broadening is mostly due to the c-axis mosaic of the graphite sample, and increases the uncertainty in the wave-vector Q measurement to about 0.05 Å^{-1}.

The TOF spectra were recorded with a multichannel analyzer (Nicolet No. 1170). The single-phonon creation and annihilation events usually show up in the TOF spectra as sharp peaks with the energy width less than 1 meV and the multiphonon scattering events as much broader peaks with the width comparable to the energy of the incident beam (17.4 meV). The position of a single-phonon peak provides the kinematic information such as phonon-dispersion relation while the line shape of the peak provides the dynamical information such as phonon density of states, inelastic-scattering cross section, and phonon lifetime. In order to obtain this information as accurately as possible, a nonlinear least-squares-fitting process was performed on some of the spectra. In doing so, we assumed that the intensity distribution of both single-phonon and multiphonon peaks can be described approximately by a Gaussian function

$$I(t)=I_o\exp[-(t-t_c)^2/2\sigma^2]\ , \tag{1}$$

where t is the flight time. For each feature, there are three fitting parameters I_o, t_c, and σ which measure the maximum, the center, and the width of the Gaussian function, respectively. The fitting function for the whole spectrum is composed of a sum of several Gaussian functions plus a constant background which represents the counting of the residual He gas in the detector chamber. The fitting process was performed on an IBM compatible personal computer (AT&T, PC6300) using the graphing software SigmaPlot (Jandel Scientific, Version 4.0). Depending on the number of fitting parameters and the number of data points, the computational time is about 0.2–2 h per spectrum. Figure 1 shows an example of the results of such a curve-fitting process. The TOF spectrum was taken from the commensurate monolayer of Kr/graphite along the $\bar{\Gamma}\bar{M}_R$ direction, which is the $\bar{\Gamma}\bar{K}$ direction of the graphite surface. Three relatively sharp peaks at 1042, 1102, and 1264 μs and a much broader multiphonon peak at 1154 μs were fitted by the sum of four Gaussian functions. As demonstrated in Fig. 1, the result of such a curve fitting is quite satisfactory. The real line shape of the inelastic-scattered intensity can be obtained by deconvoluting the fitted Gaussian function with an instrumental function, which can also be described fairly well by a Gaussian in our case.

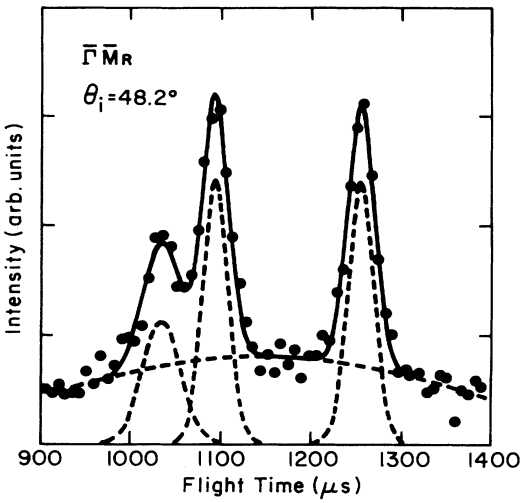

FIG. 1. An example of the curve-fitting process described in the text. The TOF spectrum is taken from the C monolayer along the $\bar{\Gamma}\bar{M}_R$ direction. Dashed lines show the individual Gaussian functions representing a single-phonon annihilation peak ($t_c=1042$ μs), a diffuse elastic peak ($t_c=1102$ μs), a creation single-phonon peak ($t_c=1264$ μs), and a multiphonon background ($t_c=1154$ μs). The solid line shows the fitted curve.

B. Growth of Kr films

The deposition of Kr films was made by exposing the sample to an effusive flow of Kr gas via a stainless-steel capillary aimed at the sample from a distance of 5–10 mm. The flow rate of Kr gas was controlled by a Varian leak valve such that the deposition rate is typically about 0.05 monolayer/min during the condensation of the first layer. Figure 2 shows a typical deposition curve obtained by measuring the surface specular reflection intensity under a constant impingement rate of Kr gas flux. The measurements were taken under nearly steady-state conditions such that the rate of change in both specular intensity and surface temperature was nearly zero. As the surface temperature is lowered, the first sharp reduction in the specular intensity is due to the monolayer condensation. As is demonstrated in the volumetric measurements,[1] the growth mode of Kr film on graphite is of the

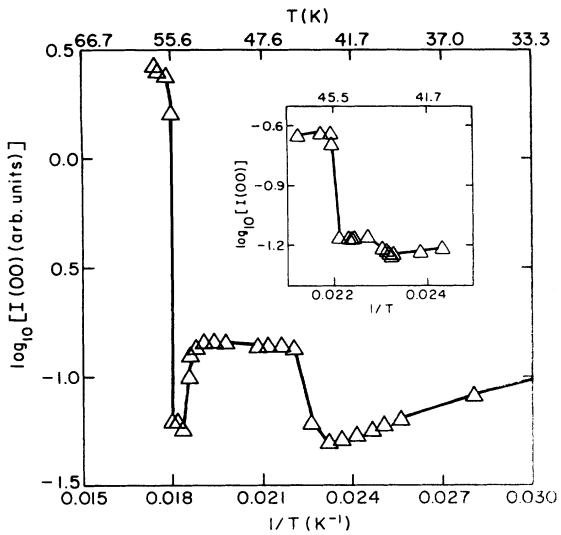

FIG. 2. Specular beam intensity during deposition of Kr on the basal plane of the graphite single crystal as the surface temperature is lowered under the constant impingement rate of Kr gas. Each point was obtained by measuring the specular intensity after a steady-state condition was reached. The inset shows the detail of the curve at temperatures near bilayer and trilayer condensation. The solid lines are a guide to the eye. See text for details.

Frank–Van der Merwe type. The adsorbate forms a commensurate $(\sqrt{3}\times\sqrt{3})R30°$ phase when the monolayer condensation is completed. The subsequent rise in the specular intensity is caused by the phase transition from the commensurate (C) phase to a hexagonal incommensurate (IC) phase, as was confirmed by measuring the diffraction beam positions. At the plateau, the compression of the incommensurate layer reaches its maximum value, which corresponds to a lattice constant of 4.04 Å or a lattice misfit of 5.3%. This dramatic rise in the specular beam intensity is quite different from that observed in the previous elastic He-atom scattering measurement, which showed a decrease in the specular beam intensity at an incident angle of 70°.[14] The difference can be interpreted as a result of the inelastic scattering at different incident angles. Further discussion of this subject is planned to be presented in a separate paper. The second- and third-layer condensation, as shown explicitly in the inset of Fig. 2, were seen upon reducing the surface temperature further. Both the lattice constant and the lattice orientation of the second and third layers are the same as those of the most compressed IC monolayer within the accuracy of our measurements. The corresponding condensation temperatures of monolayer, bilayer, and trilayer formation are estimated to be 55.5, 45.4, and 43.5±0.5 K. Below 42 K, the specular intensity increases continuously as surface temperature decreases due to the Debye-Waller effect. We do not observe any clear signature of bulk condensation, which is expected to occur at $T=40$ K based on low-energy electron diffraction (LEED), auger-electron-spectroscopy, and volumetric adsorption isotherm measurements.[17] This suggests that the physical properties, such as binding energy and vibrational energy, of third layer and bulk are nearly the same.

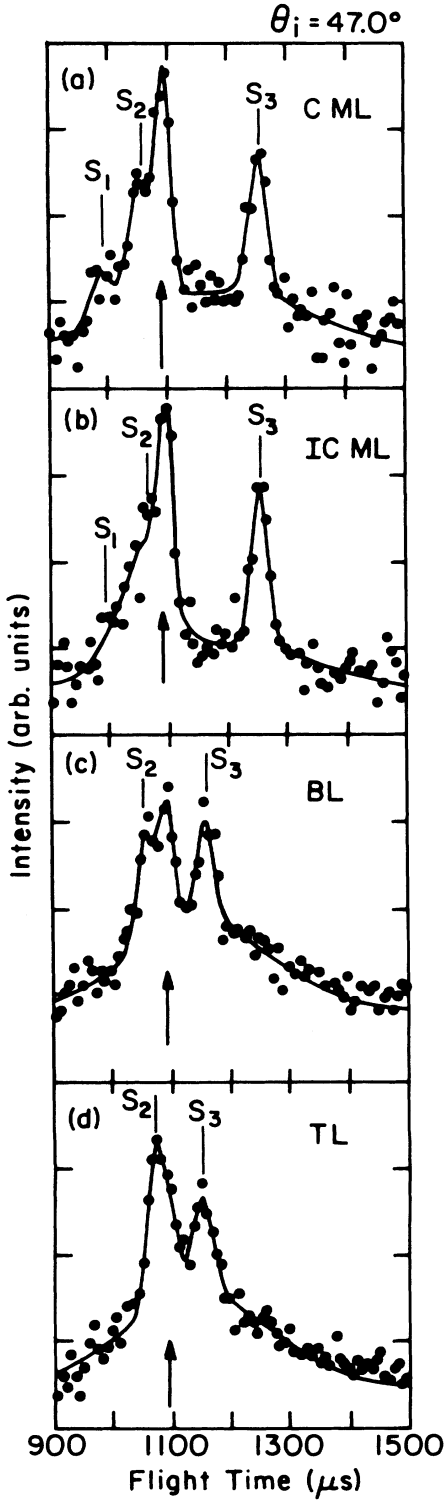

FIG. 3. TOF spectra taken from the (a) C monolayer, (b) IC monolayer, (c) bilayer, and (d) trilayer of Kr physisorbed on graphite along the $\bar{\Gamma}\bar{M}_R$ direction and at an incident angle of 47°. Each point represents the number of counts recorded by the multichannel analyzer with a channel width of 7.7 μs. Solid lines are the fitted curves and the arrows indicate the positions of the diffuse elastic peak. The positions of single-phonon annihilation ($S1$,$S2$), and single-phonon creation ($S3$) peaks are marked.

III. RESULTS

A. TOF spectra

The surface phonon measurements were performed using the technique of TOF analysis at selected coverages determined from a deposition curve like that presented in Fig. 2. In Fig. 3, we present four TOF spectra taken at $\theta_i = 47°$ for the (a) C monolayer, (b) IC monolayer, (c) bilayer, and (d) trilayer Kr films, respectively. The peaks marked by the upward arrows, observed in all four spectra, are due to diffuse elastic scattering from surface defects. The width of these peaks is about 30 μs, which corresponds to the energy width of 0.9 meV and is due mainly to the instrumental effect. The other marked peaks are due to single-phonon annihilation and creation of the $SP_\perp$ mode of the Kr films. An extended zone plot of these single-phonon features is shown in Fig. 4 along with a scan curve at $\theta_i = 47°$ and the conjectured dispersion curves of the Kr monolayer on a rigid graphite substrate. To assist further discussion, the energy transfer, phonon wave vector, the full width at half maximum (FWHM), and the integrated intensity of each single-phonon peak are also summarized in Table I. For the C monolayer, we observed one phonon-creation peak ($S3$) at -4.2 meV and two phonon-annihilation peaks ($S2$ and $S1$) at 1.4 and 3.9 meV, respectively. As can be seen from Fig. 4, $S1$ and $S3$ were observed at the positions consistent with those of the rigid-graphite-substrate approximation. In contrast, the annihilation peak ($S2$) was seen near the bulk band edge of the graphite and does not lie on the dispersion curves of the Kr monolayer on a rigid graphite substrate. Therefore the observation of the $S2$ peak is a clear indication that the Kr adatoms do not behave as Einstein oscillators. In fact, the $S2$ peak can be attributed to the effects of hybridization between the substrate Rayleigh mode and the $SP_\perp$ mode of Kr monolayer. Such effects were first predicted by the theoretical model calculations[7,18] and observed experimentally in the systems of Kr/Pt(111) and Xe/graphite.[11,12] One important difference between the system of the monolayer Kr/graphite and other systems, however, is that we saw a significant intensity tradeoff between $S1$ and $S2$. As indicated in Table I, the intensity of $S2$ peak is comparable to that of $S3$ but is much larger than that of $S1$. This fact provides evidence that the effect of the adsorbate-substrate interaction is quite strong for this system since the intensity of the $S2$ peak would be zero in the rigid-substrate approximation.

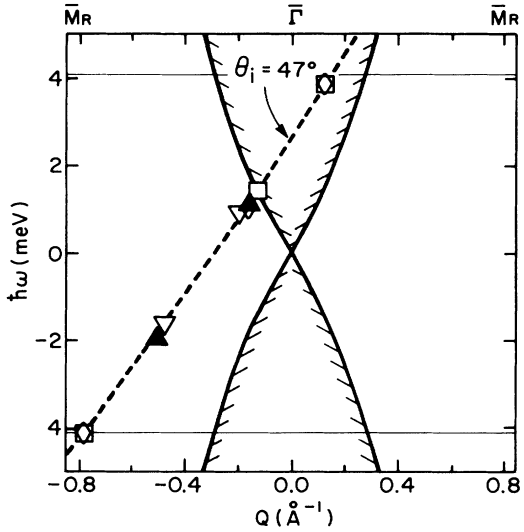

FIG. 4. Extended zone representation of the single-phonon peaks observed in the spectra in Fig. 3. Squares, diamonds, open triangles, and filled inverted triangles were taken from the C monolayer, IC monolayer, bilayer, and trilayer, respectively. The dashed line is the scan curve for $\theta_i = 47°$, solid lines are the phonon-dispersion curves of the Kr monolayer in the rigid-substrate approximation, and the shaded lines are the bulk band edge of the graphite.

For the IC monolayer, the phonon-creation peak $S3$ was observed at the same position as for the C monolayer within the accuracy of the measurements. It appears that the phonon-annihilation peaks $S1$ and $S2$ were also observed in Fig. 3(b). The positions of these peaks, as determined from the curve-fitting process, are nearly the same as for the C monolayer. This fact suggests that the lattice misfit has no apparent effect on the dispersion of the out-of-plane $SP_\perp$ mode, and is also consistent with the results of the lattice-dynamics measurements for Xe/graphite.[12]

The TOF spectrum taken from the bilayer shows a much greater change. As shown in Fig. 3(d), one creation

TABLE I. Characteristics of single-phonon peaks observed in Fig. 3. The flight time t is measured at the peak positions marked by vertical line segments in Fig. 3. Q and $\hbar\omega$ are the calculated phonon wave vector and energy. The time widths are nominal values determined directly from the fitting process while the energy widths are the true widths obtained by excluding the instrumental broadening. The intensity I, given in arbitrary units, is the integrated intensity of the each single-phonon peak. Asterisks denote quantities that cannot be determined reliably.

	C Monolayer			IC Monolayer			Bilayer		Trilayer	
Label	S_1	S_2	S_3	S_1	S_2	S_3	S_2	S_3	S_2	S_3
t (μs)	991	1053	1251	991	1063	1254	1060	1160	1070	1152
Q Å^{-1})	0.13	−0.13	−0.79	0.13	0.17	−0.79	−0.15	−0.51	−0.19	−0.48
$\hbar\omega$ (meV)	3.9	1.4	−4.2	3.9	1.1	−4.2	1.2	−1.9	0.8	−1.7
FWHM (μs)	41	43	36	*	*	35	33	32	31	43
FWHM (meV)	1.3	1.2	0.4	*	*	0.4	0.7	0.4	0.6	0.9
I (arb. units)	0.22	0.58	0.53	*	*	0.84	0.8	0.73	0.99	0.92

peak and one annihilation peak are observed at about -1.9 and 1.2 meV, respectively. Compared with the monolayer, the energy of the creation peak is reduced by 2.2 meV, which reflects the fact that the phonon-dispersion curve of the bilayer is significantly lower than that of the monolayer. In contrast to the relatively large difference between the monolayer and the bilayer, the spectrum of the trilayer is quite similar to that of the bilayer. The energy of the creation peak is at -1.7 meV while the energy of the annihilation peak at 0.8 meV, which represents only slight reductions in the phonon energies. Besides these changes in the phonon energies, a few other changes were seen as the Kr film became thicker. One was the reduction in the intensity of the diffuse elastic peak at zero energy transfer. This behavior was also seen in the system of Kr/Pt(111),[11] and indicates that the surface of a thick film is smoother than that of the thin film. The other change was the significant increase in the relative intensity of the multiphonon background in the spectra of the bilayer and the trilayer. The increase in the multiphonon background is caused partly by the fact that the surface Debye temperature of the bilayer and the trilayer is lower than that of the monolayer.

B. Dispersion curves

A total of 50 TOF spectra were taken along the $\bar{\Gamma}\bar{M}_R$ and $\bar{\Gamma}\bar{K}_R$ directions for the monolayer, and along the $\bar{\Gamma}\bar{M}_R$ direction only for the bilayer and the trilayer. The results of these measurements are plotted in Fig. 5 to show the phonon dispersion in a reduced surface Brillouin zone of the C monolayer. The phonon dispersion of the monolayer is quite similar to that of monolayer Xe/graphite.[12] Near the zone boundary, the dispersion curve is quite flat with the vibrational energy of 4.1 ± 0.1 meV, which is 0.9 meV higher than that of the Xe monolayer[12] and slightly higher than that of the slab calculation of the C monolayer Kr/graphite.[18] Approaching from the zone boundary to the zone center, the dispersion curve starts to split into two branches at approximately the same point where the extension of the flat part of the dispersion cure intersects the substrate bulk band edge. The lower branch follows the bulk band edge almost all the way to the zone center $\bar{\Gamma}$, and the upper branch is nearly flat with a much smaller change in energy as the zone center is approached. The behavior of the lower branch is quite consistent with the thin slab (13 layers) calculation of de Wette for the C monolayer Kr/graphite, but that of the upper branch seems not to agree with the calculation. According to the slab calculation, near the zone center $\bar{\Gamma}$ the adlayer mode should split into four branches. The lowest branch follows the edge of the transverse bulk band of the graphite while the other three branches lie above the bulk band edge. As discussed by Toennies and Vollmer for Xe/graphite,[12] the discrepancy is caused partially by the use of only a very thin slab of 13 layers in the calculation. Thus, the pairs of phonon modes which have different parity symmetry with respect to the mirror plane are not degenerate as they would be for a slab of infinite thickness. This causes the adlayer mode to split into four branches rather than two

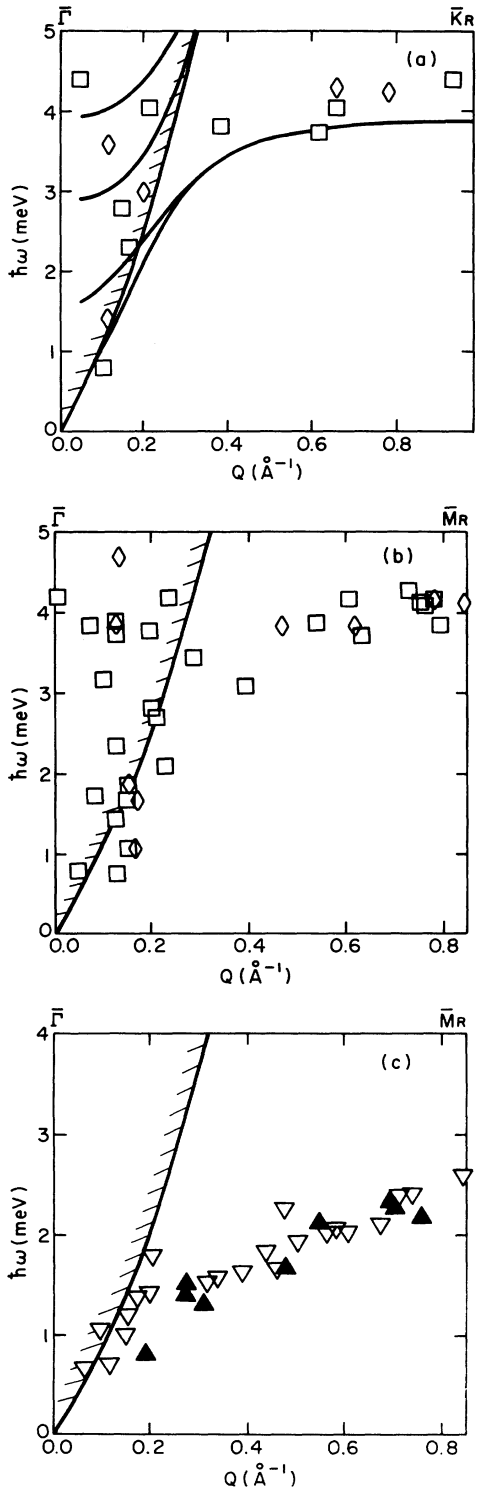

FIG. 5. Measured phonon dispersion for the Kr monolayer, bilayer, and trilayer on graphite. The measurements were taken along two principal directions: (a) $\bar{\Gamma}\bar{K}_R$ of monolayer, (b) $\bar{\Gamma}\bar{M}_R$ of monolayer, and (c) $\bar{\Gamma}\bar{M}_R$ of bilayer and trilayer. Squares and diamonds represent the C and IC monolayers, respectively, open triangles the bilayer, and filled triangles the trilayer. The solid lines in (a) are the calculated dispersion curves by de Wette *et al.* (Ref. 18) for the $SP_\perp$ mode of the Kr monolayer. The bulk band edge of graphite is indicated by shaded solid lines.

branches. The problem is avoided in the calculation of Hall, Mills, and Black for rare-gas monolayers on smooth surfaces by modeling the substrate as a semi-infinite elastic continuum.[7] This calculation predicts that an avoided-crossing behavior should occur when the adlayer mode intersects the substrate Rayleigh mode. The results of our measurements for monolayer Kr/graphite and previous measurements for monolayer Xe/graphite[12] agree qualitatively with such an avoided-crossing behavior. In spite of such an agreement, however, the calculated phonon spectral densities of the continuum model do not agree with the results of our measurements. As described earlier, we observed a significant intensity tradeoff between the $S1$ and the $S2$ peaks in the TOF spectra taken at 47°. In fact, a tradeoff pattern of similar intensity was also seen at other angles, which means that the scattered intensity from those phonons on the lower branch in Figs. 5(a) and 5(b) is much more intense than those on the upper branch. This would reflect a similar distribution in the phonon spectral density since the other factors such as the phonon energy, wavelength, and small differences in the incident angle would not affect scattered intensity significantly under the experimental conditions.[19] In comparison, the continuum model calculations show that the phonon spectral density distribution is dominated by the phonons on the upper branch, which is opposite to that of our measurements. It is interesting, however, to note that the spectral density distribution of the continuum model is consistent with the results of the inelastic He-atom scattering measurements on the monolayer Kr/Pt(111).[11] This suggests that the discrepancy is likely due to the fact that the effect of the surface corrugation was neglected in the continuum model calculation since the graphite surface is much more corrugated than the closed-packed metal surface as indicated in the atom-surface diffraction measurements.

The other important effect of adsorbate-substrate interaction, as predicted by the theory,[7] is the resonance-induced radiative damping of the adlayer phonon modes. A resonance between phonon modes of adsorbate and substrate is expected when their energies and surface projected wave vectors are the same. When in resonance, any vibrational motion of adatoms would cause the substrate to vibrate at the same frequency, and the adsorbate phonon modes would become "leaky modes" because of the energy flow from the adsorbate to the substrate. One manifestation of such a vibrational resonance is the reduction of the lifetime of adlayer phonon modes, which broadens the line shape of the single-phonon peak. This effect was confirmed in the case of Kr/Pt(111).[11] Unfortunately we cannot study this effect in detail here, mainly due to the effects of the intensity tradeoff described above. Because of such effects, the scattered intensity from the adlayer phonons, which are in resonance with those of the graphite substrate, is very weak. Therefore, the width measurements of the peaks associated with these phonons are not reliable, although the broadening of the $S3$ peak relative to $S1$ peak observed at 47° (see Fig. 3 and Table I) seems to be consistent with the picture of the resonance-induced radiative damping.

The phonon-dispersion curves of the bilayer and trilayer appear to be the same although the measurements at $\theta_i = 47°$ [Figs. 3(c) and 3(d)] indicate a small reduction of 0.2–0.4 meV in the vibrational energy as the trilayer is formed. This fact suggests that starting from the bilayer, the thickness of the Kr film has little effect on the surface phonon energy. This is consistent with the specular beam intensity measurements presented in Fig. 2 which show that only a very small intensity drop (less than 15%) was seen upon the condensation of the trilayer. It can also be seen from Fig. 5 that the dispersion curves of the bilayer and trilayer are significantly lower than that of the monolayer. The phonon energy at the zone boundary $\bar{M}_R$ is reduced to 2.5 meV, compared with 4.1 meV for the monolayer, and shows a larger dispersion as one moves toward the zone center $\bar{\Gamma}$ consistent with an increasing bulk character of the film. Accordingly, the dispersion curves of the bilayer and the trilayer would only intersect the substrate modes at an energy smaller than 1.2 meV and Q less than 0.1 Å^{-1}. Thus it would be very difficult to probe the effect of adsorbate-substrate coupling on the dispersion curve because of finite instrumental resolution in both energy and wave-vector measurements.

IV. CONCLUSION

We have presented the results of an inelastic He-atom scattering study of the lattice dynamics of the monolayer, bilayer, and trilayer Kr films on the graphite (0001) plane. The measured phonon-dispersion curve of the Kr monolayer is nearly flat for $Q > 0.3$ Å^{-1} with a vibrational energy of 4.1 meV. For $Q < 0.3$ Å^{-1}, an avoided-crossing behavior, which is due to the hybridization of the phonon modes of the adsorbate and substrate, was seen. Similar to monolayer Xe/graphite,[12] the amount of splitting in the phonon-dispersion curve due to such an avoided crossing is fairly large, indicating a rather strong adsorbate-substrate interaction. In addition, an anomalously high scattering probability of lower branch phonons was seen, which provides further favorable evidence for a strong adsorbate-substrate interaction. The lattice misfit of the Kr monolayer was found to have no apparent effect on the phonon-dispersion curve of the $SP_\perp$ mode in spite of the fact that it does change the intensity of both elastic and inelastic scattering. The overall dispersion curve of monolayer Kr/graphite is quite similar to that of Xe/graphite.[12] The dispersion curves of the bilayer and trilayer Kr appear to be the same within the accuracy of the measurements, and is considerably lower than that of the monolayer. No clear evidence of substrate effects was seen, which is due partly to the fact that the dispersion curves of the bilayer and the trilayer intersect with that of the graphite substrate only in a small ($Q \leq 0.1$ Å^{-1}) region very close to zone center $\bar{\Gamma}$.

ACKNOWLEDGMENTS

We acknowledge helpful discussions with Dr. D. Frankl, Professor M. Cole, and Professor J. Annett. This work was supported by the NSF under Grant No. DMR-8718771.

[1]A. Thomy and A. Duval, J. Chem. Phys. **66**, 1966 (1969); **67**, 286 (1970); **67**, 1101 (1970); **74**, 926 (1977).
[2]*Ordering in Two Dimensions,* edited by S. K. Sinha (Elsevier, New York, 1980).
[3]*Phase Trnsition in Surface Films,* edited by J. G. Dash and J. Ruvalds (Plenum, New York, 1980).
[4]J. G. Dash, Phys. Today **38**(2), 1100 (1985).
[5]R. J. Birgeneau and P. M. Horn, Science **232**, 329 (1986).
[6]*Phase Transition in Surface Films,* edited by H. Taub, G. Torzo, H. Lauter, and S. C. Fain, Jr. (Plenum, New York, 1991).
[7]B. M. Hall, D. L. Mills, and J. E. Black, Phys. Rev. B **32**, 4932 (1985).
[8]B. F. Mason and B. R. Williams, Phys. Rev. Lett. **46**, 1138 (1981).
[9]K. D. Gibson and S. J. Sibener, Phys. Rev. Lett. **55**, 1514 (1985); J. Chem. Phys. **88**, 7862 (1988).
[10]Klaus Kern, Rudolf David, Robert L. Palmer, and George Comsa, Phys. Rev. Lett. **56**, 2823 (1986).
[11]Klaus Kern, Peter Zeppenfeld, Rudolf David, and George Comsa, Phys, Rev. B **35**, 886 (1987).
[12]J. P. Toennies and R. Vollmer, Phys. Rev. B **40**, 3495 (1989).
[13]J. Z. Larese, W. Y. Leung, D. R. Frankl, N. Holter, S. Chung, and M. W. Cole, Phys. Rev. Lett. **54**, 2533 (1985).
[14]S. Chung, A. Kara, J. Z. Larese, W. Y. Leung, and D. R. Frankl, Phys. Rev. B **35**, 4870 (1987).
[15]J. Cui, D. R. Jung, and D. R. Frankl, Phys. Rev. B **42**, 9701 (1990).
[16]B. D. Weaver and D. R. Frankl, Rev. Sci. Instrum. **59**, 92 (1988).
[17]S. C. Fain, Jr. and M. D. Chinn, J. Phys. (Paris) Colloq. **38**, C4-99 (1977); A. Thomy, J. Regnier, and X. Duval, in *Thermochimie,* Colloques Internationaux du CNRS (CNRS, Paris, 1972), Vol. 201, p. 511; Y. Larher, J. Chem. Soc. Faraday Trans. If**70**, 320 (1974); G. L. Pollack, Rev. Sci. Instrum. **40**, 577 (1969).
[18]F. W. de Wette, B. Firey, E. de Rouffignac, and G. P. Alldredge, Phys. Rev. B **28**, 4744 (1983).
[19]H. Ibach and T. S. Rahman, in *Chemistry and Physics of Solid Surfaces V,* edited by R. Vanselow and R. Howe (Springer-Verlag, Berlin, 1984), p. 455.